A WIDE BANDWIDTH MODEL FOR THE ELECTRICAL IMPEDANCE OF MAGNETIC BEARINGS

David C. Meeker
Eric H. Maslen
Myounggyu D. Noh
Department of Mechanical, Aerospace, and Nuclear Engineering
University of Virginia
Charlottesville, VA

SUMMARY

Magnetic bearings are often designed using magnetic circuit theory. When these bearings are built, however, effects not included in the usual circuit theory formulation have a significant influence on bearing performance. Two significant sources of error in the circuit theory approach are the neglect of leakage and fringing effects and the neglect of eddy current effects. This work formulates an augmented circuit model in which eddy current and flux leakage and fringing effects are included. Through the use of this model, eddy current power losses and actuator bandwidth can be derived. Electrical impedance predictions from the model are found to be in good agreement with experimental data from a typical magnetic bearing.

INTRODUCTION

Maxwell's equations are generally adequate to describe the magnetic and electric fields inside a magnetic bearing. It is possible to approximately solve Maxwell's equations directly using the finite element method [1] [2] [3]. However, the computational cost of a 3-D eddy current solution is very high. Moreover, the effects of any particular design parameter may be difficult to isolate in such an elaborate model.

It is common to develop a simplified magnetic circuit analysis for design using the assumptions

- no flux fringing, or spreading out of the flux in the vicinity of air gaps in the bearing.
- no flux leakage, or flux that circulates locally around a coil through unmodeled paths.
- negligible eddy current effects
- flux density uniform in every flux-carrying cross-section

NOMENCLATURE

a	Cross-sectional area of flux path.	m	number of poles in stator.
A	Magnetic vector potential.	M	Air gap influence matrix.
B	Magnetic flux density.	n	Number of turns in coil.
b	Frequency domain magnetic flux density.	p_k	k^{th} pole in the expansion of μ_{fd}.
		r	Magnetic reluctance.
$\mathbf{B}$	Vector magnetic flux density.	s	Laplace variable.
d	Lamination thickness.	V	Voltage.
$\mathbf{E}$	Vector electric field intensity.	w	Axial length of magnetic bearing.
H	Magnetic field intensity.	z_k	k^{th} zero in the expansion of μ_{fd}.
$\mathbf{H}$	Vector magnetic field intensity.	α	$(\omega\sigma\mu d^2/2)$
I	Coil current.	ζ	$\sqrt{\sigma\mu}d/2$
j	$\sqrt{-1}$	μ	Magnetic permeability.
J	Current density.	σ	Electrical conductivity.
$\mathbf{J}$	Vector current density.	ϕ	magnetic flux.
l	length of flux path section.	ω	excitation frequency.
L	Inductance matrix.	$\Delta\Omega$	Magnetomotive force drop.

by which Maxwell's equations are reduced to a set of circuit equations [4]. The magnetic field can then be determined by solving a relatively small set of linear algebraic equations. The resulting magnetic circuit theory is commonly used in the design of magnetic bearings. However, the presence of leakage, fringing, and eddy current effects can lead to significant discrepancies between circuit theory predictions and experimental performance.

The objective of this work is to present an augmented magnetic circuit model that accounts for the effects of eddy currents, leakage, and fringing in magnetic bearings without abandoning the circuit paradigm. The development will be directed specifically towards the case of active radial magnetic bearings, as pictured in Figure 1. Corrections for eddy currents are developed from a 1-dimensional eddy current model often employed for losses in transformer cores. Extra leakage paths are proposed to account for the effects of flux leakage, and a magnetostatic finite element model is used to correct the reluctance of the air gaps for fringing effects and to identify the reluctance of leakage paths. Bearing electrical impedance predicted by the augmented circuit model is compared to experimental measurements and to predictions made using the usual circuit techniques. In this comparison, the augmented model predicts the experimental results more accurately than typical circuit methods.

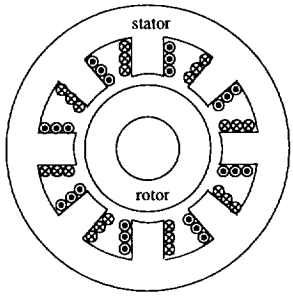

Figure 1: Active radial magnetic bearing.

RELATED WORK

A one-dimensional eddy current formulation for laminated magnetic circuits has been available since Stoll [5]. This formulation has been used more recently in several instances to analyze eddy current losses in transformers [6] [7] [8]. However, the one-dimensional analysis has not been applied to cores with complicated connectivity. Zmood [9] applied a one term expansion of the formulation in [5] to a simple magnetic bearing. The present work extends Zmood's formulation so that a bearing with an arbitrarily complex network of flux paths can be addressed with an expansion of arbitrary order.

Previous works have accounted for fringing effects at the pole tips in magnetic bearings by isolating the tip regions from the rest of the bearing and solving magnetic scalar potential in the region of the air gap [10] [11]. In these analyses, the iron is assumed to be infinitely permeable; it can then be treated solely by defining a constant value of magnetic scalar potential at the iron-air interface. The air gap reluctance deduced from this infinite permeability solution is then assumed to apply in a magnetic circuit with high (but not infinite) iron permeability.

These previous works, however, dealt with geometries in which the pole tips could be conveniently isolated from the geometry of the rest of the bearing. In a typical radial magnetic bearing, the ends of the poles are not so removed from the rest of the bearing structure as to allow an examination of the pole in isolation from the rest of the bearing. This work presents a general infinite permeability method of determining air gap reluctance based on magnetic vector potential that uses the solution of the field in all sections of the air between the rotor and stator to determine fringing corrections. In this process, the forms of additional leakage paths are suggested, and the reluctances of these leakage paths can be determined.

EDDY CURRENT CORRECTION

The use of a one-dimensional eddy current model to describe eddy currents in thin laminations has been addressed in the literature. As reported in Stoll [5], the effects of

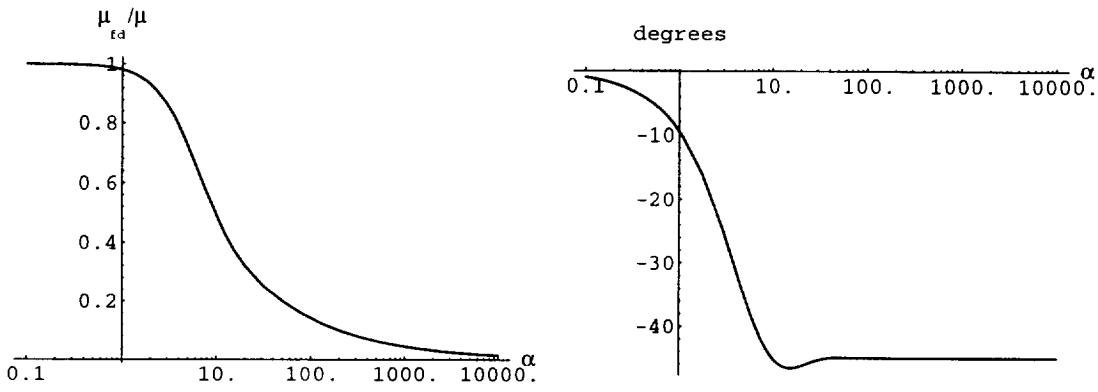

Figure 2: Magnitude and phase shift of $\mu_{fd}(j\omega)$ versus frequency.

eddy currents can be incorporated into a frequency-dependent permeability, $\mu_{fd}(s)$:

$$\mu_{fd}(s) = \mu \left[\frac{\tanh(\sqrt{s\sigma\mu}\,\frac{d}{2})}{\sqrt{s\sigma\mu}\,\frac{d}{2}} \right] \tag{1}$$

where d is lamination thickness, σ is conductivity, and μ is steady-state permeability. Permeability μ_{fd} can be used in magnetic circuit equations in a way analagous to regular permeability: magnetomotive force drop across a section of laminated iron is

$$\Delta\Omega(s) = \frac{l}{\mu_{fd}(s)}\bar{b} \tag{2}$$

where $\bar{b}$ is the average flux density in the laminated section.

If harmonic response is desired, $\mu_{fd}(j\omega)$ can be evaluated at any particular ω. Permeability $\mu_{fd}(j\omega)$ can be evaluated in terms of standard functions:

$$\mu_{fd}(j\omega) = \mu \left[\frac{(1 - e^{-2\sqrt{\alpha}} + 2e^{-\sqrt{\alpha}} \sin\sqrt{\alpha}) - j\,(-1 + e^{-2\sqrt{\alpha}} + 2e^{-\sqrt{\alpha}} \sin\sqrt{\alpha})}{\sqrt{\alpha}\,(1 + e^{-\sqrt{\alpha}} + 2e^{-\sqrt{\alpha}} \cos\sqrt{\alpha})} \right] \tag{3}$$

where

$$\alpha = \frac{\omega\sigma\mu d^2}{2} \tag{4}$$

The magnitude variation and phase shift of $\mu_{fd}(j\omega)$ are shown Figure 2. Once $\mu_{fd}(j\omega)$ is obtained, magnetic circuit analysis then proceeds with a complex permeability for the iron sections of flux path.

However, a model that remains in the Laplace domain is a necessary prerequisite for the use of many tools from control theory. If (1) is simply substituted into the set of circuit equations in symbolic form, solving the magnetic circuit equations becomes laborious. Instead, the magnetomotive force drop across a laminated section can be defined as

$$\Delta\Omega(s) = \frac{l}{\mu}\bar{b} - I_e(s) \tag{5}$$

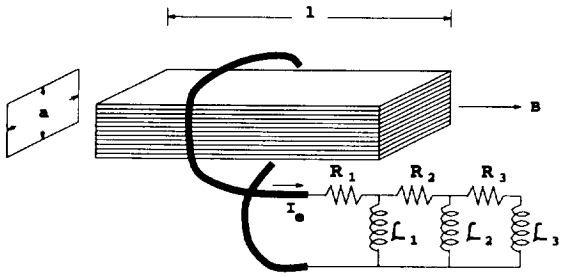

Figure 3: Equivalent circuit model for eddy currents.

From a magnetic circuit standpoint, I_e is merely a 1-turn coil wound around the laminated section of interest that carries some arbitrary current, just like the regular pole windings. The electric circuit equations for each pole winding are then written assuming that all I_e's are arbitrary inputs to the system. The current flowing in I_e is then determined by the transfer function

$$\frac{I_e(s)}{\phi(s)} = \left[\frac{l}{a\,\mu} - \frac{l}{a\,\mu_{fd}(s)}\right] \tag{6}$$

where $\phi = \bar{b}\,a$ is the total flux flowing through the laminated section. The hyperbolic tangent can be expanded in continued fraction form as [7]:

$$\tanh x = \cfrac{x}{1 + \cfrac{x^2}{3 + \cfrac{x^2}{5 + \cdots}}} \tag{7}$$

which can be substituted into (6) to yield

$$\frac{I_e(s)}{\phi(s)} = -\left(\frac{l}{\mu\,a}\right) \cfrac{s\gamma^2}{3 + \cfrac{s\gamma^2}{5 + \cdots}} \qquad \text{where} \quad \gamma = \sqrt{\sigma\mu}\frac{d}{2} \tag{8}$$

With some algebraic manipulation, (8) can be re-arranged in the form

$$\frac{I_e(s)}{\phi(s)} = \cfrac{-s}{R_1 + \cfrac{1}{\frac{1}{s\mathcal{L}_1} + \cfrac{1}{R_2 + \cfrac{1}{\frac{1}{s\mathcal{L}_2} + \cdots}}}} \tag{9}$$

where

$$\mathcal{L}_i = \frac{\mu\,a}{(4i+1)\,l} \tag{10}$$

$$R_i = \frac{4\,(4i-1)a}{\sigma l d^2} \tag{11}$$

Equation (9) can be interpreted as the transfer function of a one-turn coil driving the chain of resistors and inductors pictured in Figure 3. The effects of eddy currents can be viewed as a parasitic winding around each section of iron flux path that drives a chain of resistors and inductors. For a finite state model, the chain is simply truncated after an arbitrary number of resistor-inductor pairs.

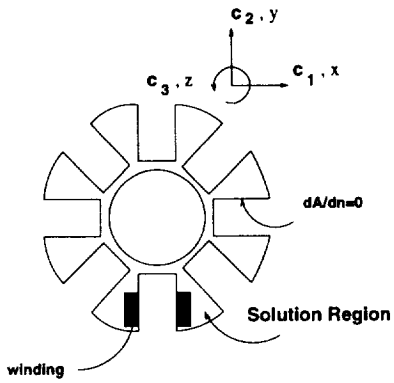

Figure 4: 2-D solution region inside a magnetic bearing.

LEAKAGE AND FRINGING CORRECTIONS

To determine an adequate network of bulk flux paths and to solve for the reluctance of the air sections in those circuit paths, the coupled coil inductances derived from a magnetostatic field solution will be compared to the inductances derived by circuit techniques. In both cases, inductance will be determined with μ of the iron in the bearing assumed to be infinity. The reluctances derived (for $\mu = \infty$) are assumed to apply for a finite but high permeability material with eddy current effects.

If a bearing is suitably long in the axial direction, axial end effects can be neglected; a 2-dimensional analysis is then sufficient to determine leakage and fringing effects. In a 2-D model, vector potential is related to flux by

$$\mathbf{B} = \frac{\partial A}{\partial y}\mathbf{c}_1 - \frac{\partial A}{\partial x}\mathbf{c}_2 \tag{12}$$

where $x, y, \mathbf{c}_1$, and $\mathbf{c}_2$ refer to Figure 4. Following the development in [12], the magnetostatic field satisfies the differential equation

$$\nabla^2 A = J \tag{13}$$

where J is the coil current density flowing in the $\mathbf{c}_3$ direction.

A great simplification in the solution of (13) is to assume that the iron in the solution region is infinitely permeable. The boundary condition

$$\nabla A \cdot \mathbf{n} = 0 \tag{14}$$

then applies at the air-iron interface where $\mathbf{n}$ is a vector normal to the interface. The field then need not be computed inside the iron sections.

In a radial magnetic bearing, the solution region assuming infinite iron permeability is then limited to the air between the rotor and stator. If the stator is symmetric and the rotor is

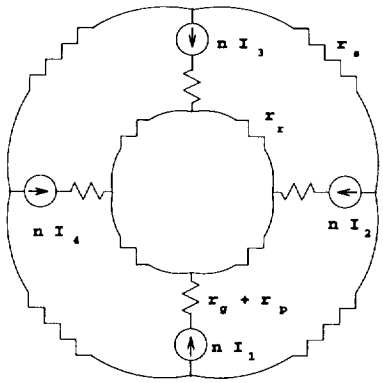

Figure 5: Equivalent circuit model of a 4 pole symmetric radial magnetic bearing.

centered, all possible flux distributions for any set of coil currents can be determined by the superposition of the solutions found with only one active coil. Such a solution domain is pictured in Figure 4 for an 8-pole radial magnetic bearing. It is then relatively straight-forward and economical to solve for A inside the air and coils using the finite element method [12].

Once the A field is determined inside the air and coils of the bearing, the mutual inductance between the i^{th} and j^{th} coils (denoted $\hat{L}_{ij}$) can be determined by the integration [13]:

$$\hat{L}_{ij} = w\frac{\iint A_i J_j \, dx \, dy}{I_i I_j} \tag{15}$$

In this integration, A_i is the contribution to A from current in the i^{th} coil, J_j is the current density contribution of the the j^{th} coil, I_i and I_j are the currents flowing in the i^{th} and j^{th} coils respectively, and w is the axial length of the bearing. The integration is taken over the entire solution domain, but the only non-zero contributions to the integral are in the area of the j^{th} coil.

Note that inductance is computed by (15) without assuming any network structure for the flux. A set of magnetic circuits must be deduced such that when the air gap reluctances in that circuit model are appropriately chosen, the circuit theory inductance closely matches the field theory inductance as $\mu \to \infty$.

The nominal equivalent circuit model used in radial magnetic bearings is pictured in Figure 5. For simplicity, a four pole symmetric radial bearing is shown instead of the usual eight-pole bearing. Symbols r_p, r_r, and r_s correspond to the reluctances in the iron of the pole, rotor, and stator respectively. These reluctances are computed from the formula

$$r = \frac{l}{\mu_{fd}(s)a} \tag{16}$$

where l corresponds to the length and a to the cross-sectional area of the segment in

question. Reluctance r_g is the air gap reluctance and has a nominal value of

$$r = \frac{l_g}{\mu_o a_g} \tag{17}$$

without the inclusion of fringing effects. The flux in any part of the bearing can be deduced by analogy to electric circuits where magnetic reluctance corresponds to electrical resistance and magnetic flux to electrical current [4].

In the circuit model, the inductance between the i^{th} and j^{th} coils (denoted L_{ij}) is

$$L_{ij} = n \frac{\partial \phi_i}{\partial I_j} \tag{18}$$

where ϕ_i is the flux passing through the i^{th} coil, I_j is the current in the j^{th} coil, and n is the number of turns in the j^{th} coil.

In the infinite permeability case, reluctances due to iron (r_r, r_s, and r_p) are all zero. For a symmetric bearing, the self inductance of each coil is

$$L_{ii} = \frac{m-1}{m}\left(\frac{n^2}{r_g}\right) \tag{19}$$

and the mutual inductance is

$$L_{ij} = \frac{-1}{m}\left(\frac{n^2}{r_g}\right) \qquad i \neq j \tag{20}$$

At this point, air gap reluctance r_g could be chosen to minimize the difference between corresponding entries in circuit theory inductance matrix L and field theory inductance matrix $\hat{L}$. However, the existence of error between L and $\hat{L}$ that cannot be eliminated by the proper choice of r_g suggests that extra leakage flux paths exist and should be modeled. In the nominal circuit model, all flux produced by a coil returns to that coil by eventually passing through another coil on the stator. The summation of the entries of any row of L is therefore zero. The sum of the row entries in $\hat{L}$, however, is generally non-zero; some of the flux travels in loops not accounted for by the usual circuit model. The chief cause of this discrepancy is a self-leakage path for each coil. Some flux makes a complete circuit flowing only in the air and iron immediately adjacent to an active coil and never crosses the air gap to link with other coils. Leakage mutual inductances also exist, but these mutual leakage paths are usually an order of magnitude more reluctant than the self-leakage path and can be neglected with little error incurred.

Fortunately, a self-leakage path is simple to incorporate into the nominal circuit model. This leakage is a short circuit path that loops around a coil without passing through the bulk reluctances associated with the pole iron and the air gap for the corresponding leg. This path is visualized in Figure 6, where r_l signifies the reluctance of the leakage path.

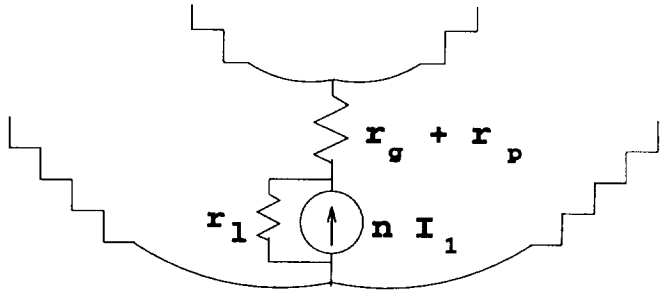

Figure 6: Equivalent circuit for self-leakage path.

Some parts of the leakage flux travel through the iron in the leg and stator adjacent to the coil of interest. However, the reluctance of the air part of the bulk leakage path is very large; the increase in the reluctance of the leakage path due to finite permeability in the iron is arguably negligibly small in comparison. The leakage flux is therefore idealized as flowing only in the coil itself and in the air around it from a circuit standpoint.

The fluxes in the gaps are identical with and without the self-leakage path; an extra flux of

$$\phi_{leak} = \frac{n}{r_l} I_i \tag{21}$$

is merely added to the flux that passes through the i^{th} coil. The only effect is to increase the self-inductance of a coil:

$$L_{ii} = \frac{m-1}{m}\left(\frac{n^2}{r_g}\right) + \frac{n^2}{r_l} \tag{22}$$

Off-diagonal terms in L remain the same as before. An over-determined set of linear equations can now be solved for r_g^{-1} and r_l^{-1} by equating L and $\hat{L}$. If the bearing is symmetric, it is sufficient to compare only the first row of L and $\hat{L}$. Denoting the first row of L as L_1, row L_1 can be decomposed as:

$$L_1' \equiv M \left\{ \begin{array}{c} r_g^{-1} \\ r_l^{-1} \end{array} \right\} \text{ where } M = \left[\begin{array}{cc} n^2\left(\frac{m-1}{m}\right) & n^2 \\ \frac{-n^2}{m} & 0 \\ \vdots & \vdots \\ \frac{-n^2}{m} & 0 \end{array} \right] \tag{23}$$

The least-squares solutions for the gap and leakage reluctances are then

$$\left\{ \begin{array}{c} r_g^{-1} \\ r_l^{-1} \end{array} \right\} = [M'\,M]^{-1}\,M'\,\hat{L}_1' \tag{24}$$

POWER LOSS AND ACTUATOR BANDWIDTH CALCULATION

A frequency-dependent bearing inductance can be obtained either by the use of $\mu_{fd}(s)$ in inductance calculation or by measurement of bearing electrical impedance. Once this inductance is determined, power loss and actuator bandwith can be deduced by relatively simple calculations.

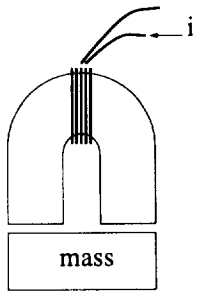

Figure 7: Simple magnetic actuator.

Power Loss

At a given frequency ω, inductance L can be separated into real and imaginary components:

$$L(j\omega) = L_r + j\,L_i \tag{25}$$

where L_r and L_i are both real numbers. In the frequency domain, the voltage drop across the bearing is

$$V(j\omega) = j\omega\,(L_r + j\,L_i)I(j\omega) \tag{26}$$

Eq. (26) implies that if the current going through a bearing is

$$I(t) = i\,\sin\omega t \tag{27}$$

the voltage drop across the bearing is

$$V(t) = \omega\,i(-\,L_i\,\sin\omega t + L_r\,\cos\omega t) \tag{28}$$

Noting that instantaneous power loss is $I(t)\,V(t)$, the power loss can be integrated through one cycle and divided by the cycle length to yield average power loss:

$$\text{Power Loss} = -\frac{\omega}{2}\,L_i\,i^2 \tag{29}$$

In the absence of eddy currents, L_i is zero. When eddy currents are modeled, L_i is a negative number, resulting in a power loss.

Actuator Bandwidth

Determination of actuator bandwidth will be addressed by considering a simple example; however, the method is readily extended to more complicated actuators. Specifically, consider the actuator shown in Figure 7. A single horseshoe electromagnet pulls a mass upwards against the force of gravity. The force, f, produced by this bearing is

$$f(t) = \frac{1}{\mu_o\,a}\,(\phi_b + \phi_p)^2 \tag{30}$$

pole length	l_p	0.0181 m
pole area	a_p	1.210×10^{-4} m^2
air gap length	l_g	4.572×10^{-4} m
air gap area	a_g	1.210×10^{-4} m^2
stator length	l_s	0.0366 m
stator area	a_s	1.210×10^{-4} m^2
rotor length	l_r	0.0198 m

rotor area	a_r	0.786×10^{-4} m^2
lam. thickness	d	0.635×10^{-3} m
conductivity	σ	$9.017 \times 10^6\,(\Omega \cdot \mathrm{m})^{-1}$
permeability	μ	$5000\,\mu_o$
turns	n	76 turns/pole
coil resistance	R_c	0.62 Ω
shunt resistance	R_s	15.35 Ω

Table 1: Kingsbury Bearing Dimensions

where ϕ_b is a constant bias flux and ϕ_p is perturbation flux. If ϕ_b is chosen to exactly counteract gravity and the magnitude of ϕ_p is assumed small, the net force on the mass is

$$f(t) \approx \frac{1}{\mu_o\, a}\phi_b\phi_p \tag{31}$$

Perturbation flux $\Phi_p(s)$ is related to perturbation current $I_p(s)$ by

$$\Phi = \frac{L(s)}{n} I_p \tag{32}$$

implying that the relation between force and current in the Laplace domain is

$$F(s) = \left(\frac{\phi_b}{\mu_o\, a\, n}\right) L(s)\, I_p(s) \tag{33}$$

From eq. (33), it can be concluded that the bearing bandwidth is identical to the bandwidth of the frequency-dependent inductance.

EXPERIMENTAL COMPARISON–FREQUENCY RESPONSE

To test the accuracy of the augmented circuit methods, performance predictions made using the circuit method were compared to experimental results from an 8-pole radial bearing made by **Kingsbury, Inc.** The dimensions of this bearing are described in Table 1. For testing purposes, only one leg of the stator is wound with a 76-turn coil.

A two-dimensional finite element analysis of the bearing and coil was performed. Since the bearing and all windings are symmetric, it is sufficient to consider only the first row of $\hat{L}$, denoted $\hat{L}_1$. The first entry in this row corresponds to the self-inductance of the test coil, and the other entries in the row correspond to the mutual inductances that would be obtained if identical coils lay on each of the other legs. The following $\hat{L}_1$ was obtained by the finite element model:

$$\hat{L}_1' = \{2.0069, -0.2772, -0.2735, -0.2732, -0.2729, -0.2732, -0.2735, -0.2772\} \text{ mHenries}$$

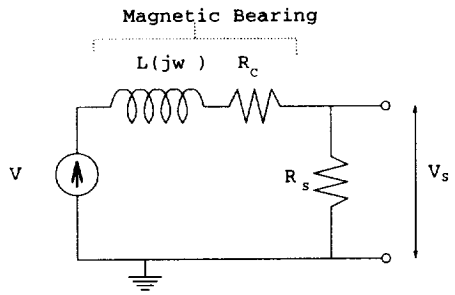

Figure 8: Test circuit.

Solving for r_g and r_l via (24) yields

$$r_g = 2.631 \times 10^6 \ \frac{\text{Wb}}{\text{A}} \qquad\qquad r_l = 6.701 \times 10^7 \ \frac{\text{Wb}}{\text{A}}$$

For comparison purposes, the air gap reluctance predicted by the nominal magnetic circuit model without leakage and fringing corrections is

$$r_{g,nominal} = \frac{l_g}{\mu_o g} = 3.007 \times 10^6 \ \frac{\text{Wb}}{\text{A}} \tag{34}$$

Fringing effects reduce the predicted air gap reluctance by 12.5 percent relative to the nominal reluctance. Leakage effects add another 0.086 mH of inductance, amounting to 4.30 percent of the total predicted self-inductance including leakage and fringing corrections when $\mu = \infty$.

Reluctances of the iron sections are computed from (16):

$$r_p = \frac{l_p}{\mu_{fd} a_p} = \frac{150.0\,\text{m}^{-1}}{\mu_{fd}} \qquad r_s = \frac{l_s}{\mu_{fd} a_s} = \frac{298.8\,\text{m}^{-1}}{\mu_{fd}} \qquad r_r = \frac{l_r}{\mu_{fd} a_r} = \frac{249.4\,\text{m}^{-1}}{\mu_{fd}} \tag{35}$$

For any particular frequency of interest, $\mu_{fd}(j\omega)$ is evaluated via (3).

The test bearing is included in a measurement circuit as pictured in Figure 8. Resistance R_c is the intrinsic resistance of the wire in the bearing's coil. Resistance R_s is an arbitrarily chosen current shunt resistance. In the present case, a 15.35 Ω resistor was employed. The input to the circuit is the voltage V. The measured output of the circuit is the voltage V_s. The transfer function of the electric circuit model is

$$\frac{V_s}{V} = \frac{R_s}{s\,L(s) + (R_s + R_c)} \tag{36}$$

The test bearing was subjected to a sine wave sweep varying from 100 Hz to 10^5 Hz. The output signal was convolved with the input signal to determine the magnitude and phase shift of the output.

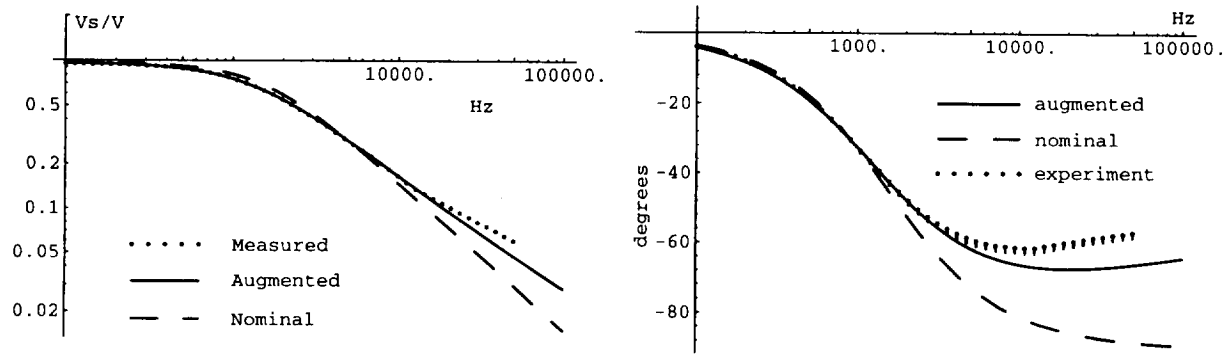

Figure 9: Frequency response of test circuit.

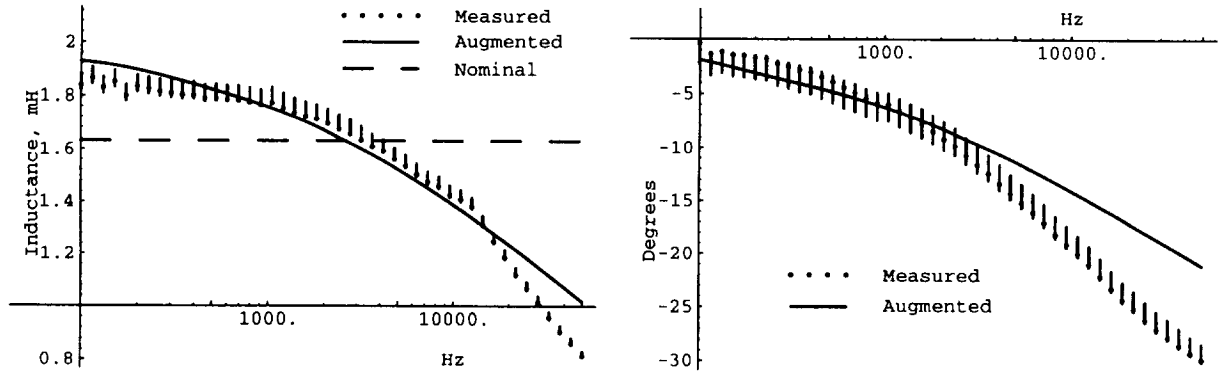

Figure 10: Response of frequency-dependent inductance.

A direct comparison of the measured transfer function $\frac{V_s}{V}$ can now be made with the transfer functions predicted by the augmented circuit model and the nominal circuit model. Figure 9 is a comparison of predicted and measured frequency response of test circuit. By substituting experimentally measured values of V_s/V into (36), one can solve for the frequency-dependent inductance of the bearing. Experimentally derived and predicted $L(j\omega)$ are compared to the nominal magnetic circuit model inductance in Figure 10. In each figure, the error bars associated with the measured data represent the maximum deviations expected due to experimental uncertainty.

At low frequencies (less than 1000 Hz), eddy current effects are negligible; the differences between the augmented and nominal models are due solely to leakage and fringing effects. In this frequency region, the augmented model shows an improvement in predictive accuracy over the nominal model. The nominal model underestimates the inductance in this region, but the corrected gap and leakage reluctances yield an inductance at low frequency that closely agrees with the experimentally derived inductance. The augmented

model also correctly predicts the "corner frequency" at which the magnitude response suddenly decreases; the nominal model over-predicts the corner slightly.

At higher frequencies, eddy currents become a significant effect. Figure (10) shows that a significant drop in inductance is predicted by the augmented model at higher frequencies. Experiment verifies this drop. Most significantly, eddy currents induce a recovery in phase in a situation where a simple inductor model predicts a terminal phase lag of 90^o as $\omega \to \infty$. The augmented model predicts the recovery of phase fairly well, with some loss of accuracy at the highest frequencies considered. Discrepancies between the augmented model and experiment at high frequency could be due to any of several effects:

- a breakdown in the accuracy of the leakage and fringing model due to a low effective permeability,
- capacitive effects in the test coil,
- saturation effects caused by concentration of flux near the sides of the lamination,
- mechanical resonance effects in the test apparatus.

An interesting phenomenon predicted by the augmented model is a terminal phase lag of 45^o. This result is possible because of the infinite number of poles and zeros associated with $\mu_{fd}(s)$. Far out on the negative real axis, poles and zeros are placed increasingly close together (on a log scale) to yield a terminal 45^o lag. The experiment corroborates this prediction.

CONCLUSIONS

An augmented magnetic circuit model was presented to account for eddy current, leakage, and fringing effects in radial active magnetic bearing. Although leakage and fringing corrections are derived from a bearing model in which the iron is assumed infinitely permeable, a good correspondence with experimental data was observed when these correction factors were applied to a model with complex iron permeability. The eddy current corrections, derived from a 1-D eddy current model, were also found to adequately account for a drop in bearing inductance with frequency. The eddy current correction can be evaluated at a specific frequency when frequency response is desired, or truncated into a finite-state model for use in transient response calculations or control applications. In both instances, a structure of arbitrarily complicated connectivity can be addressed. In summation, the augmented magnetic circuit model provides an improvement in the prediction of bearing performance over usual circuit methods without resorting to computationally expensive 2-D or 3-D finite element eddy current models.

REFERENCES

[1] Carpenter, C. J.: Comparison of Alternative Formulations of 3-Dimensional Magnetic-Field and Eddy-Current Problems at Power Frequencies. *Proc. IEE*, vol. 124, no. 11, Nov. 1977, pp. 1026-1034.

[2] Biro, O.; and Preis, K.: On the Use of Magnetic Vector Potential in the Finite Element Analysis of Three-Dimensional Eddy Currents. *IEEE Trans. Mag.*, vol. MAG-25, no. 4, July 1989, pp. 3145-3159.

[3] Williamson, S.; and Chan, E. K. C.: Three-Dimensional Finite Element Formulation for Problems Involving Time-Varying Fields, Relative Motion, and Magnetic Saturation. *IEE Proc-A*, vol. 140, no. 2, Mar. 1993, pp. 121-130.

[4] Plonus, M.: *Applied Electromagnetics.* McGraw-Hill, 1978.

[5] Stoll, R. L.: *The Analysis of Eddy Currents.* Oxford University Press, 1974.

[6] Avila-Rosales, J.; and Alvarado, F.: Nonlinear Frequency Dependent Transformer Model for Electromagnetic Transient Studies in Power Systems. *IEEE Trans. PAS*, vol. PAS-101, no. 11, Nov. 1982, pp. 4281-4288.

[7] Tarasiewicz, E. J. *et al.*: Frequency Dependent Eddy Current Models for Nonlinear Iron Cores. *IEEE Trans. Power Systems*, vol. 8, no. 2, May 1993, pp. 588-597.

[8] de Leon, F.; and Semlyen, A.: Time Domain Modeling of Eddy Current Effects for Transformer Transients. *IEEE Trans. Power Delivery*, vol. 8, no. 1, Jan. 1993, pp. 271-280.

[9] Zmood, R. B.; Anand, D. K.; and Kirk, J. A.: The Influence of Eddy Currents on Magnetic Actuator Performance. *Proc. IEEE*, vol. 75, no. 2, 1987, pp. 259-60.

[10] Walowit, J. A.; and Pinkus, O.: Analytic and Experimental Investigation of Magnetic Support Systems. Part 1: Analysis. *J. of Lubrication Technology*, vol. 104, July 1982, pp. 418-428.

[11] Tuschiya, K. *et al.*: Anisotropic Stiffness Effect of Stability of a Magnetically Suspended Momentum Wheel. *J. of Guidance, Control, and Dynamics*, vol. 14, no. 2, pp. 330-336.

[12] Hoole, S. R.: *Computer-Aided Analysis and Design of Electromagnetic Devices.* Elsevier, 1989.

[13] Rogers, W. E.: *Introduction to Electric Fields, A Vector Analysis Approach.* McGraw-Hill, 1954.